YF Baranov et al.

Accumulation trend of heavy impurities in the core of Neutral Beam and ICRF heated plasmas in JET

Accumulation trend of heavy impurities in the core of Neutral Beam and ICRF heated plasmas in JET.

Yu.F.Baranov[1], F.Casson[1], C. Challis[1], G.Corrigan[1], V. Goloborodko [2,3], P. Jacquet[1], E.Lerche[1,4] , M.O'Mullane[5] , V.Parail[1], S. Sharapov[1] and JET contributors*

EUROfusion Consortium, JET, Culham Science Centre, Abingdon, OX14 3DB, UK
[1]*CCFE, Culham Science Centre, Abingdon, OX14 3DB, UK*
[2] *Institute for Nuclear Research, Ukrainian Academy of Sciences, Prospect Nauki 47, 03680, Kiev, Ukraine.*
[3] *Institute for Theoretical Physics, University of Innsbruck, Association EUROfusion-OEAW, Technikerstr. 25, 6020, Innsbruck, Austria.*
[4]*LPP-ERM-KMS, TEC partner, 1000 Brussels, Belgium*
[5]*Department of Physics, University of Strathclyde, Glasgow, G4 0NG, UK*

* see the Appendix of F. Romanelli et al., Proceedings of the 25th IAEA Fusion Energy Conference 2014, Saint Petersburg, Russia

Abstract

Strong accumulation of heavy impurities has been observed in the core of JET plasmas with ITER-like wall (ILW). A database has been created to analyse experimentally observed trends. Well pronounced dependence between the core plasma radiation, heavy impurity content and normalised scaling factor $S = C\omega^2 n_D / T^{3/2}$ has been found in NB heated plasmas, where ω, n, T and C are the plasma rotation frequency, density, temperature and a constant, respectively. The dependence is distorted in the plasmas with combined neutral beam injection (NB) and ion cyclotron (RF) heating due to large additional influx of the heavy metal impurities from the wall. The radiation becomes more peripheral in the plasmas with combined heating. Three major factors cause the difference between NB only and NB plus RF heated plasmas: stronger density and weaker temperature peaking and faster toroidal rotation in NB only heated plasmas. The experimental trends can be partly explained by the neoclassical theory applicable to heavy impurities in the presence of a strong toroidal rotation.

Introduction. Radiation peaking has been observed in the core of JET plasmas with the ILW [1],[2],[3],[4]. The radiation peaking is associated with the accumulation of tungsten primarily and to a lesser extent to lighter impurities such as nickel, copper and chromium [1],[2],[3],[4],[5]. In hybrid plasmas, the tungsten accumulation correlates with excitation of MHD and confinement degradation [1]. In high power NB heated plasmas the tungsten accumulation may cause significant radiation cooling of the plasma core and also cause confinement degradation. In some cases the radiation collapse is observed with a subsequent disruption. Three independent processes contribute to the accumulation of impurities in the plasma centre: (i) the plasma wall interaction, responsible for the source of the impurity particles [7], (ii) the penetration of the impurities through the edge transport barrier ([1],[8]) and (iii) diffusive-convective transport in the plasma core [1],[2],[3]. The impurity source due to the plasma wall interaction and its transport in the divertor and the scrape-off layer has been analysed [8] using 1.5D core (from magnetic centre to separatrix) and 2D Scrape-Off-Layer (SOL) code JINTRAC [9]. The importance of the neoclassical convection and diffusion across the edge transport barrier has been emphasised and modelled in [1],[8]. The neoclassical effects in the presence of the toroidal rotation and poloidal asymmetry have been explored for a description of the impurity transport in the plasma core [10],[11],[12],[13],[14],[15],[16]. A combination of the neoclassical and anomalous transport has been investigated using the drift-kinetic code NEO [12] and the gyrokinetic code GKW [17],[18].

A database has been created to analyse empirical trends of the plasma radiation associated with accumulation of heavy impurities in JET plasmas with ILW. This investigation is focussed on the baseline scenario plasmas with NB and RF heating. Strong plasma rotation in the presence of high power NB heating creates poloidally asymmetric

2

distribution of the heavy impurities in the main plasma density. Such asymmetry causes a significant modification of the neoclassical transport of the impurities, compared to the non-rotating plasmas. In particular, large inward convective velocity may cause a strong accumulation of the impurities in the plasma core [12],[13],[14],[15],[16] and enhanced radiation . The impurity convection depends mainly on the relation between plasma density, temperature and toroidal rotation profiles. The database has been created to trace such relations as observed in the experiment.

In this paper, we reported a correlation between heavy impurity accumulation in the plasma core and a parameter called the scaling factor $S=C\omega^2 n_D/T^{3/2}$, representing a combination of the plasma toroidal rotation and impurity-ion collision frequency dependence on the plasma density and temperature. The characteristics of such correlation have been described. A link between plasma density and temperature peaking, R/L_n and R/L_T, toroidal rotation and the scaling factor has been traced, where R is the major radius and $R/L_F = F/(dF/dR)$. A difference between NB heated plasmas and plasmas with combined NB and RF heating has been analysed. The distinctive features of density, temperature and rotation profiles in pulses with different heating were demonstrated. The paper is structured as follows: the results of the database analysis and qualitative comparison with prediction based on the neoclassical theory presented in section 1. A difference in the transport properties of pulses with different heating methods causing a distinctive features of the impurity accumulation is demonstrated in section 2. The results are summarised in last section Discussion and Conclusions.

1. Relation between plasma radiation and the main parameters in JET baseline scenario plasmas with ILW.

To demonstrate qualitatively the effect of the main plasma parameters on the radiation caused by heavy impurity accumulation we first consider, as an example, JET-ILW pulses with very similar plasma conditions (differences will be highlighted). The evolution of the main plasma parameters is shown in Fig.1 for two pulses with combined NB+RF heating (#85266) and NB only (#85267) heating. The total heating power, plasma density, diamagnetic energy and β_N are very similar in these pulses. The total plasma bulk radiation measured by a bolometry is 15-20% larger in the pulse with combined NB and RF heating (#85266). Nitrogen gas puff starts at 12s in both pulses shown in Fig.1. Nitrogen impurity causes increase in the plasma confinement associated with the increase in the pedestal temperature and density. Simultaneously, the impurity influx causes the rise in peripheral and total radiation with time delay of about 0.2s. The effect of the confinement improvement and total radiation increase associated with nitrogen seeding can be seen in pane (d) and pane (e), respectively. The plasma radiation is measured by vertical and horizontal bolometer cameras. The radiation profiles measured by the cameras are shown in Fig.2 as a function of the angle between the axis along the major radius and the line of sight. The radiation signals from the divertor region have been suppressed in the graph. It is useful to characterise the radiation of the bulk of the plasma by the radiation signals from the plasma core and periphery. Channels 14 and 18 of the horizontal camera set have been chosen for this purpose as shown in Fig.1, Fig2 and Fig.3. Channels 3-5 from the vertical camera characterize the radiation profile skewness in the direction of the major radius as shown in Fig.2b and 3. The time averaged radiation measured in horizontal channels 18 and 14 are compared in Fig.1 for the both pulses in panes f and g, respectively. The radiation peaking is represented by the ratio of Prad(ch14)/Prad(ch18) and compared for the pulses in the pane h. One can make a conclusion that the level of the total (Fig.1,e) and the line integrated peripheral radiation (Fig.1,f) is

4

higher in the pulse 85266 after a start of RF heating (Fig.1,b), practically, until the end of this phase, but the peaking of the radiation profile increases with time and reaches the very high value of 14 in a pulse with NB heating only (Fig.1,h, Fig.2). Very effective radiation cooling reduces the plasma core temperature and causes a disruption in the pulse.

The toroidal plasma rotation profiles have been measured in some pulses by the Charge Exchange (CX) diagnostic. When available the measured rotation frequency from CX is in a good agreement with rotation frequency of the 1/1 mode in the vicinity of the q=1 surface, which has been deduced from magnetic probe measurements. The q=1 surface is close to the magnetic axis at r/a ≈0.1-0.2. The rotation frequency from the magnetic probes is shown in pane (i) of Fig.1. An important observation is the fact that the rotation frequency is smaller in pulse with combined NB+RF compared to NB heated pulse. The difference in the toroidal rotation can be ascribed to either a difference in torque due to the difference in NB power (see Fig.1 b) and/or to some other factors, which will be discussed later and may have important consequences for the process of tungsten and radiation peaking.
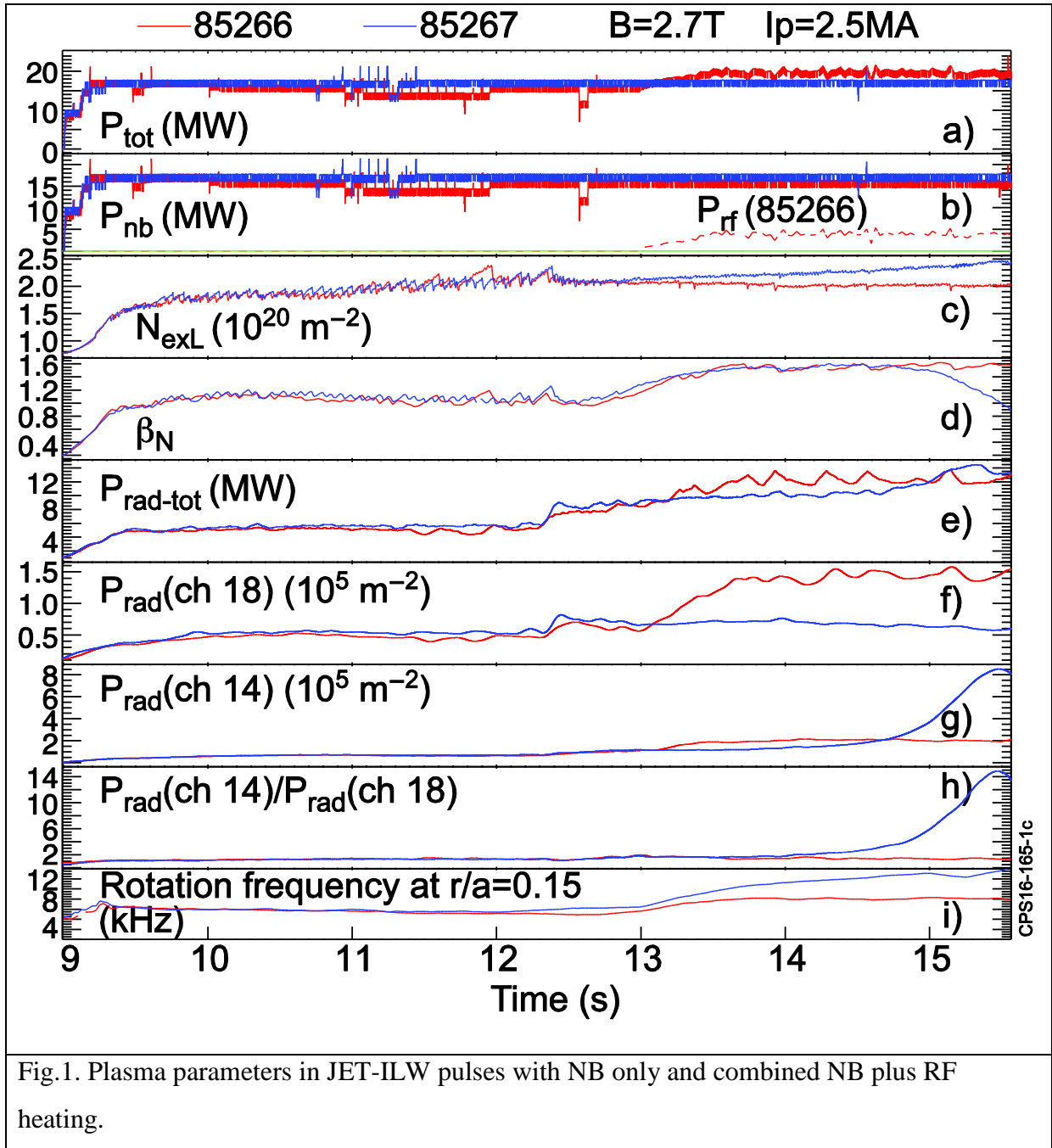
Fig.1. Plasma parameters in JET-ILW pulses with NB only and combined NB plus RF heating.

The low vs high field side asymmetry of the radiation profiles is well pronounced in Figs.2b. It is certainly connected to the large fraction of trapped W ions f_{tr}. The trapped ions are localised in the low field side in the presence of the toroidal rotation. At a lower rotation frequency (#85266) the asymmetry is modest, but it increases with time as the rotation frequency increases (see Fig.1i and Fig2b). It is important to note that large increase in the radiation and impurity concentration peaking during the pulse occur mainly due to

6

redistribution of the impurities already accumulated in the plasma core and not due to influx of additional impurities from the plasma edge. Indeed, a strong increase in the radiation peak at t=55.3s for pulse 85267 with NB only heating is accompanied by a visible reduction of the radiation in the peripheral channels as compared to the earlier time t=52.5s for the same pulse (see Fig.2). In both pulses the maximum of the radiation is shifted towards the low field side during the pulse, however it remains relatively peripheral in the case of the combined heating (#85266) while it moves towards magnetic axis in NB only heated plasma

A significant increase in the rotation frequency occurred in pulse 85267 between these two time slices. It is accompanied by a considerable increase in the radiation peaking associated with large convective velocity of heavy impurities V_r. On the contrary, no visible increase in the peaking factor (Fig.1h and Fig.2a) can be seen in pulse 85266 with combined RF and NB heating. There was also no increase in the toroidal rotation frequency between the two time slices in this pulse (Fig.1i).
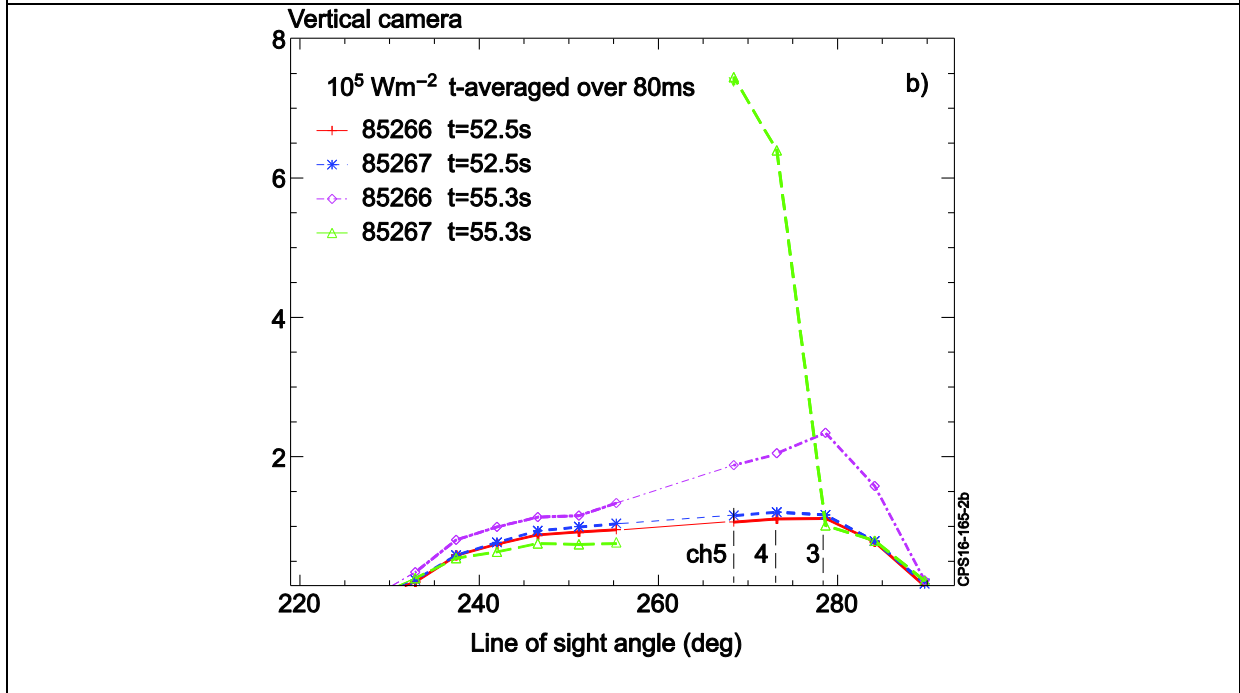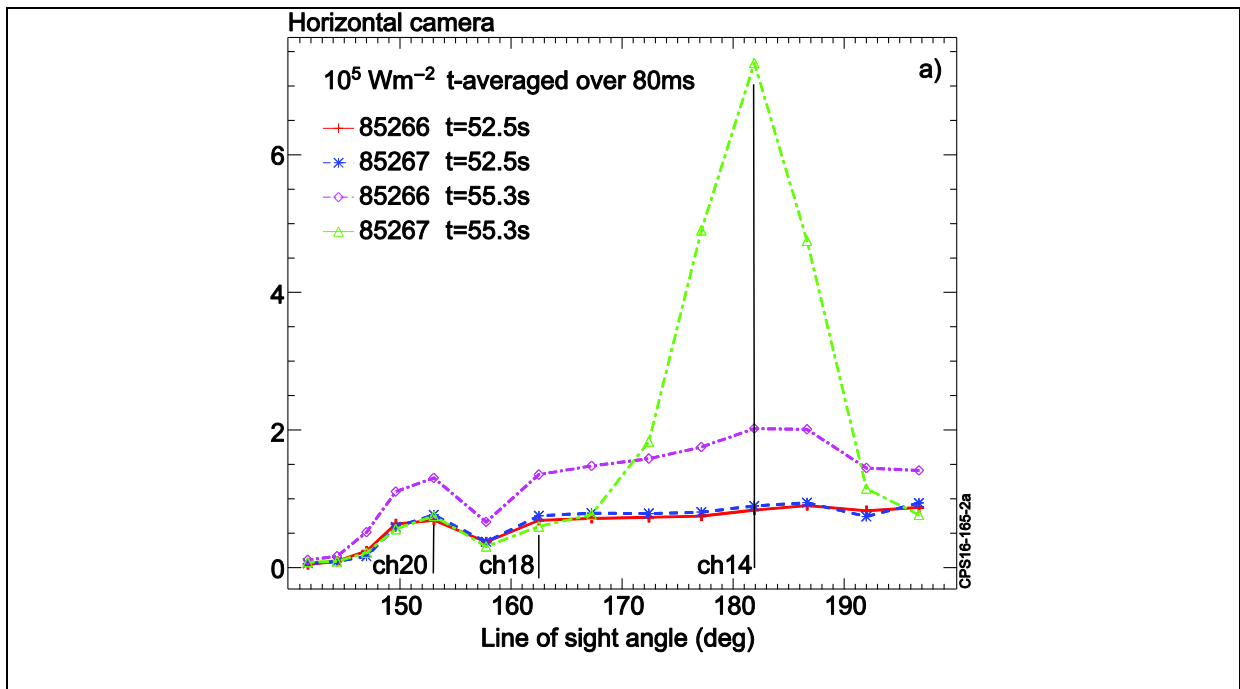
Fig.2 (a) Radiation profiles measured by horizontal (a) and vertical (b) bolometer cameras. Positions of lines of sight corresponding to marked signals are shown in in (b) Vertical camera signals from the divertor between 256° - 267° have been removed. Interpolated signals in this region are shown by thinner lines. They approximately represent the total line integrated radiation minus radiation from the divertor radiation. Interpolation of signal for #85267 at t 55.3s is not representative. It is not shown. Lines of sight nearest to the magnetic axis are shown in both figures.

Fig.3 Position of lines of sight for bolometer camera in the poloidal plasma cross-section.
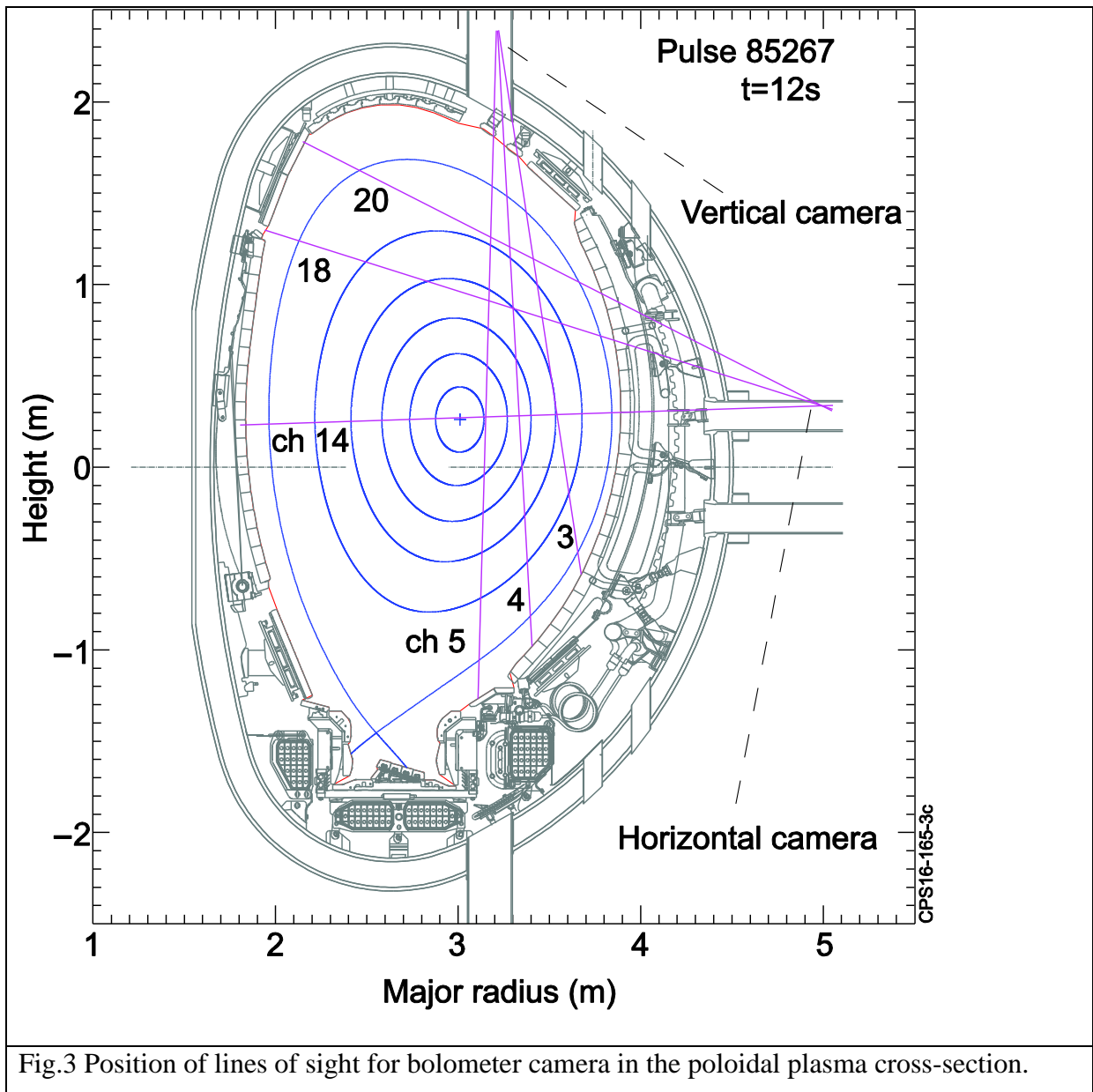
A database has been created to identify the plasma parameters linked to the radiation peaking due to heavy impurity accumulation. The database includes parameters from the baseline scenario pulses with regular ELMs, sawtooth activity, line averaged density above $5.10^{19} m^{-3}$ at the plasma current $I_p > 2.4MA$ and $P_{NB} > 14MW$. The rotation frequency was deduced from the magnetic measurement of the 1/1 mode frequency. This frequency is close to the frequency of the plasma toroidal rotation in the vicinity of the magnetic axis at r/a~0.1-0.2 and it is in a good agreement with the measured plasma rotation from CX, where available. The data were selected every half second in the heating phase with NB power $P_{nb} > 14MW$. The steady state is not reached in some pulses, especially in cases with strong impurity accumulation. Due to such selection the database demonstrates trends, partly reflecting the evolutionary processes.

A relation between the normalised scaling factor S=
$(\omega_0 / 10 \times 2\pi)^2 (N_{eL} / 2.10^{20} m^{-2}) / T_v^{1/5} (keV)$ and parameter $P_r = P_{rad}(ch14)/P_{rad}(ch18)$ (see Fig.2, Fig.3), characterising the radiation peaking is shown in Fig.4. The central rotation frequency f_0 varies between 5 and 20 kHz in the database presented in Fig.4. The line integrated density N_{el} reasonably represents the average plasma density as in the baseline scenario plasmas the pedestal density is not significantly different from the averaged density. The ion temperature T_D of the main species (deuterium) is not available in every pulse from the database. For that reason the volume averaged electron temperature T_v have been used as an estimate for the volume averaged T_D. The data are shown in Fig.4 for pulses with and without Nitrogen seeding. There is no significant difference in effective plasma charge Z_{eff} for both groups of pulses, and $Z_{eff} < 1.7$ in all pulses from the database. The plasma dilution is relatively small at such low Z_{eff}. There is a noticeable scatter of the points in Fig.4. Partly the scatter can be ascribed to different heating powers (see later) and boundary conditions

associated with different plasma configurations such as position of the strike-points and the X-point in the divertor, plasma wall distance. All these factors may affect an impurity influx.

The dependence of the peaking factor P_r on the normalised scaling factor S reflects a dependence of the ratio $V_r a / D_r$ on S, where V_r and D_r are the convective velocity and impurity diffusion coefficient, respectively, and a is the minor radius. The factor P_r should be greater for larger $|V_r a / D_r|$ and for the same plasma parameters including boundary conditions. However, the JET-ILW plasmas rarely reach steady state in the case of large peaked core radiation. Varying plasma parameters and boundary condition in the database do not allow to define V_r, D_r or $V_r a / D_r$ dependence on the scaling factor S. Nevertheless, Fig.4 allows to conclude that S is a good ordering parameter to characterise the radiation peaking P_r. It should be noted that the scatter in Fig.4 can be ascribed to the transient processes in non-steady state plasmas and to the variation in the plasma boundary conditions in addition to already mentioned factors.

The RF heating was successfully applied in JET to prevent W accumulation in the core of the ELMy H-mode plasmas [19]. The ratio of P_{rf}/P_{nb} has been used as a parameter defining the colour coding in Fig.4. The P_{RF} varies in the database between 0 and 6MW. The highest value of normalised scaling factor S and f_0 are reached in pulses with NB only heating. On the contrary, lower values of these parameters have been observed in pulses with the largest ratio P_{RF}/P_{NB}. It should be noted that for given values of P_{NB} and plasma density smaller rotation frequencies are generally observed in pulses with larger P_{RF}/P_{NB}.
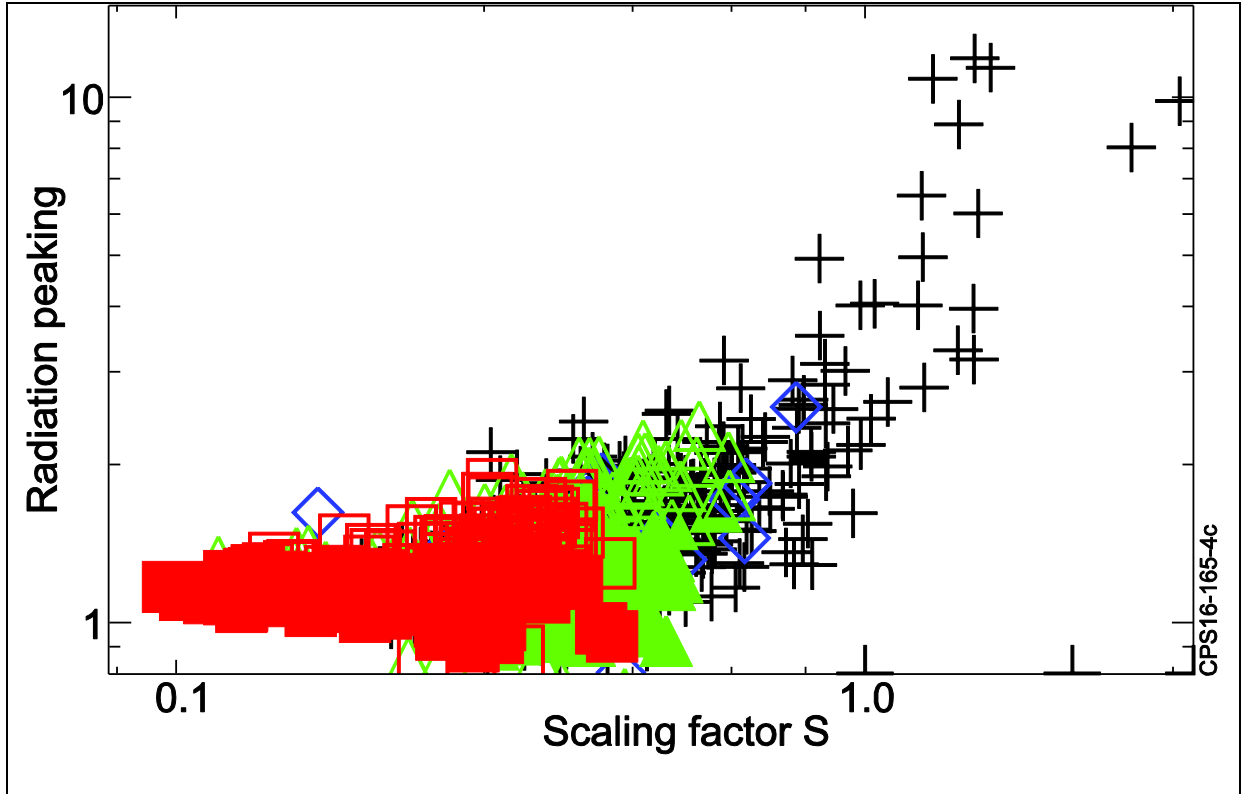
Fig.4. Radiation peaking= Prad(ch 14)/Prad(ch 18) vs. normalised scaling factor S= $(\omega_0 / 10 \times 2\pi)^2 (N_{eL} / 2.10^{20} m^{-2}) / T_v^{1/5} (keV)$, where central rotation frequency $f_0 = \omega_0 / 2\pi$, N_{el}- line integrated plasma density, $T_v^{3/2}$ -volume averaged temperature. Colour coding: black crosses- $P_{RF}/P_{NB}<5\%$, blue diamonds- $5\%<P_{RF}/P_{NB}<10\%$, green triangles- $10\%<P_{RF}/P_{NB}<20\%$, red squares- $20\%<P_{RF}/P_{NB}$. The database includes plasmas, at $B_0>2.7T$ and $I_p>2.4MA$, $P_{NB}>14MW$.

The ratio of the plasma bulk radiation to the total heating power Rt=Prad(bulk)/($P_{rf}+P_{nb}$) rises as the scaling factor S increases, as shown in Fig.5a. Due to impurity accumulation the ratio Rt approaches 1 in pulses without RF heating. However, in the range of comparable S factors, relatively higher ratio Rt is observed in pulses with additional RF heating compared to NB only heating and it increases with the P_{RF}/P_{nb} ratio. Such difference occurs due to considerable increase in the peripheral radiation in pulses with additional RF heating as shown in Fig.5b.

A dominant part of the bulk radiation is from W ions in NB only heated plasmas [1],[5]. When applying ICRF heating some other impurities are also detected via spectroscopy, in particular Ni, Cu. Fig.6a and Fig.6.b show a count rate of emission of Ni26

and CU27 ions versus normalised scaling factor S. Clear pronounced trend can be seen for large values of the factor S corresponding to the plasma with NB only heating. This trend is similar to the behaviour of the radiation peaking in Fig.4 and the radiation fraction in Fig.6a. The trend is obscured in the plasma with additional RF heating due to significant change in the influx of the impurities from the wall.

The rise of the radiation peaking, radiation fraction $Rt = Prad(bulk)/(P_{rf} + P_{nb})$ and the line emission of heavy impurities in pulses with NB heating only, in a similar way, can be explained by enhanced convection of the heavy metal impurities. The relative increase in the radiation fraction Rt and the peripheral radiation (see Fig.5b) in pulses with the combined heating compared to NB only heating can be explained by increase in the source of heavy metal particles at the edge due to plasma wall interaction, reported earlier [20]. Thee ration R_t increases with the rise of P_{RF}/P_{NB} power [20].
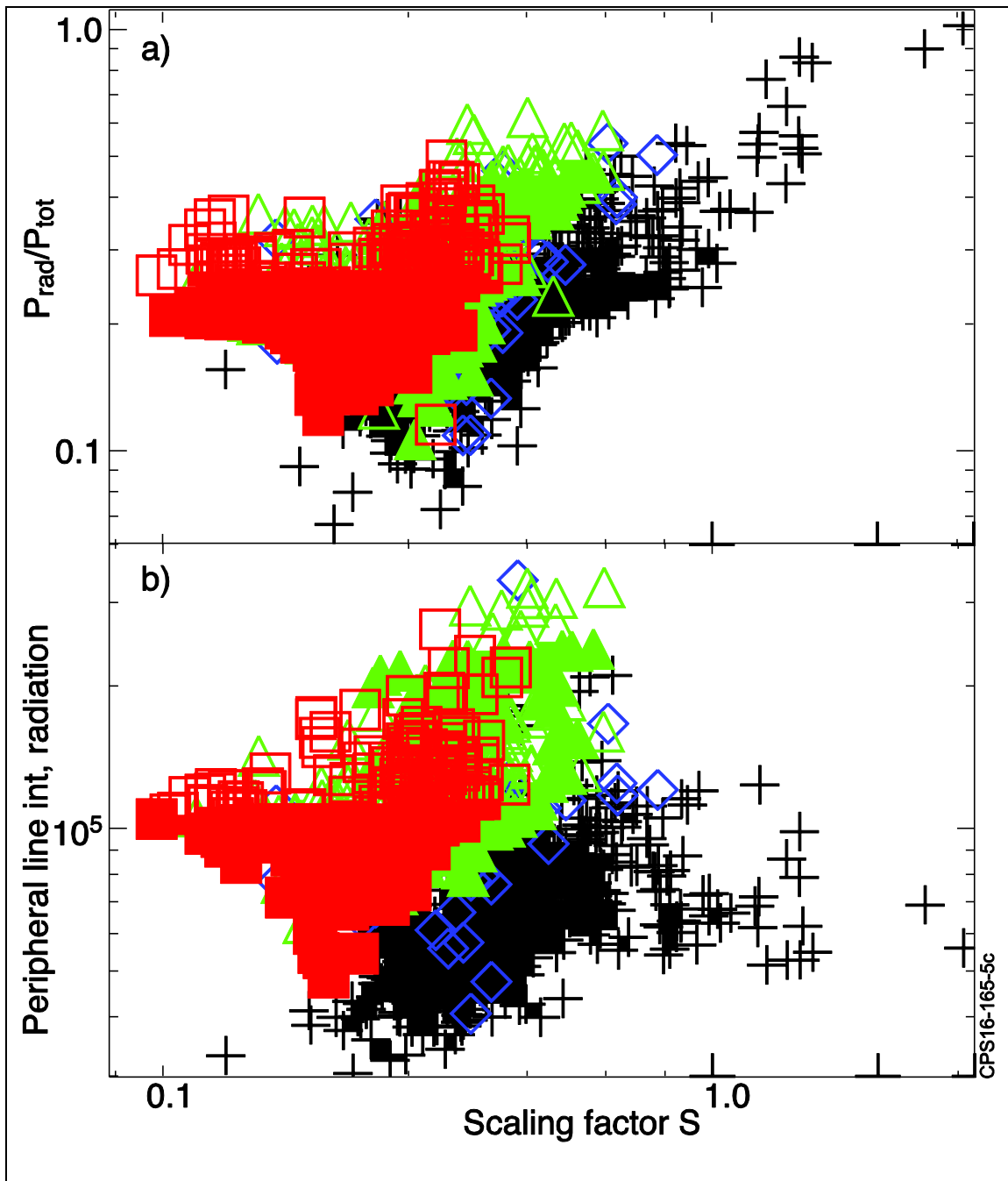
Fig.5. a) Rt=Prad(bulk)/(P$_{rf}$+P$_{nb}$) vs. normalised scaling factor S, b) line integrated radiation measured by bolometer in Ch.18 (see Fig.3) vs. S. Parameter is the ratio P$_{RF}$/P$_{NB}$. Colour coding as in Fig.4.Colur coding as in Fi.13: black crosses-P$_{RF}$/P$_{NB}$<5%, blue diamonds- 5%<P$_{RF}$/P$_{NB}$<10%, green triangles- 10%<P$_{RF}$/P$_{NB}$<20%, red squares- 20%<P$_{RF}$/P$_{NB}$.

14

Fig.6. Emission of line a) CU27 and b) NI26. Parameter is the ratio P_{RF}/P_{NB}. Colour coding as in Fig.4: black crosses-$P_{RF}/P_{NB}<5\%$, blue diamonds- $5\%<P_{RF}/P_{NB}<10\%$, green triangles-$10\%<P_{RF}/P_{NB}<20\%$, red squares- $20\%<P_{RF}/P_{NB}$.

15

The relation between the plasma bulk radiation, the radiation peaking and plasma energy confinement time τ_E is shown in Fig.7. The highest energy confinement time in the database $\tau_E = 0.3 - 0.35$ has been reached, mainly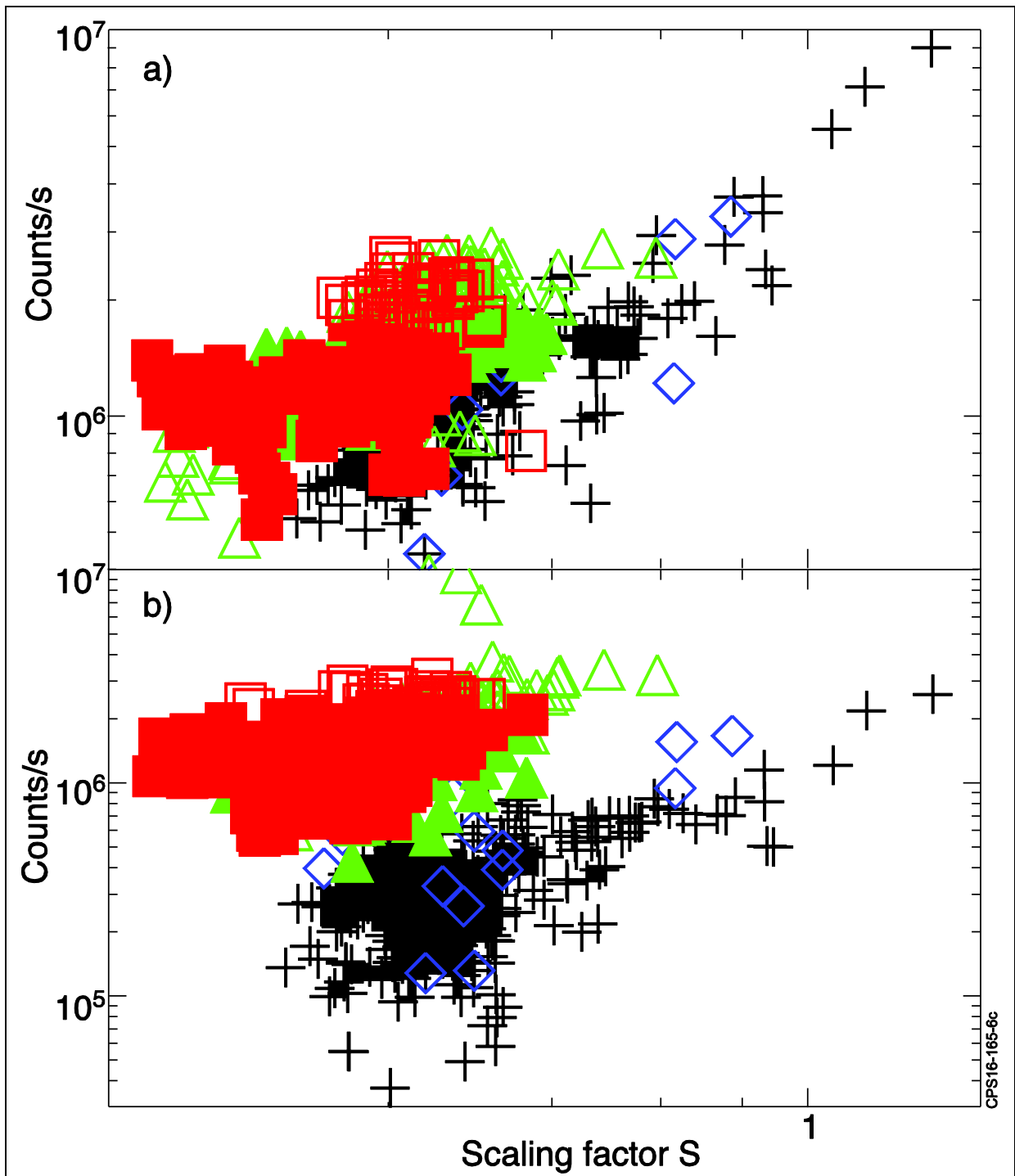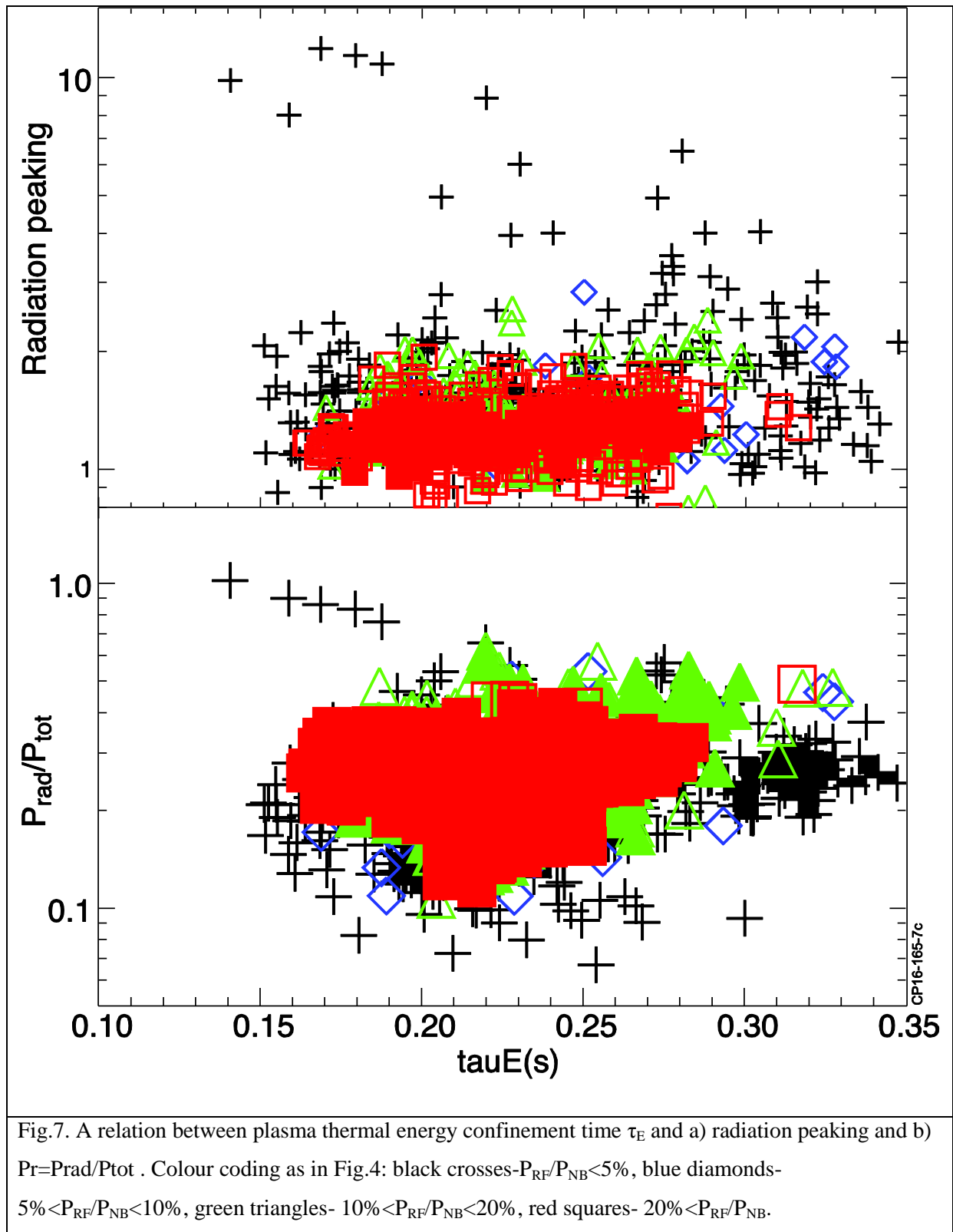, in pulses with NB only heating or pulses with a small ratio P_{RF}/P_{NB} <10% at relatively low radiation peaking factor <2 and ratio of Prad/Ptot<50%. With the rise of radiation peaking factor the radiation fraction increases and energy confinement decreases to a low value of 0.1-0.2s, when the radiation peaking approaches 10 (Fig.7a). It happens when the scaling factor S tends to its maximum value around 20 and the ratio Pt=Prad(bulk)/(Prf+Pnb)~1 (see Fig.5a). A significant drop in τ_E occurs when the core radiation becomes comparable to the total plasma heating in the case of NB heated plasmas. In such cases the pulses evolve through the radiative collapse to a disruption. The confinement time τ_E on average is smaller in pulses with combined heating with larger ratio of P_{RF}/P_{NB}>10% (see Fig.7b). The radiation fraction in such pulses remains below 0.6 in overwhelming majority of cases. In such pulses the radiation losses do not cause the radiation collapse. It should be noted that τ_E can be slightly overestimated in Fig.7 for pulses with RF heating as the calculation of τ_E requires the thermal plasma energy $W_{th} = W_{dia} - 3/2 W_{\perp fast}$, where W_{dia} is the measured diamagnetic energy and $W_{\perp fast}$ is the perpendicular component of the fast particle energy. In the presence of RF the energy of the fast particles might be underestimated. The error in the $W_{\perp fast}$ increases with P_{RF} and can reach 15%.

.

16

Fig.7. A relation between plasma thermal energy confinement time τ_E and a) radiation peaking and b) Pr=Prad/Ptot . Colour coding as in Fig.4: black crosses-P_{RF}/P_{NB}<5%, blue diamonds-5%<P_{RF}/P_{NB}<10%, green triangles- 10%<P_{RF}/P_{NB}<20%, red squares- 20%<P_{RF}/P_{NB}.

A link between the relative density and temperature peaking p_N/p_T and scaling factor S is shown in Fig.8. The density peaking $p_N=N_e(R_0)/N_e(R_1)$ and the temperature peaking $p_T=Te(R_0)/Te(R_1)$ were deduced from the Thomson scattering, where R_0=3.05m is close to the

17

magnetic axis radius and $R_1=3.4$m. The smallest density and largest temperature peaking is observed in pulses with combined heating at the smallest factors S and at the largest ratio of P_{RF}/P_{NB}. The reduction in p_N/p_T can be, partly, explained by additional central RF heating. In contrast, in NB only heated plasmas p_N/p_T ratio can reach values of 1 or higher partly due to larger radiation cooling and more peripheral heating. Some common features can be observed in dependences of the radiation peaking (Fig.13) and relative peaking p_N/p_T (Fig.8) on the scaling factor S. The strongest radiation and impurity peaking occurs in pulses with largest p_N/p_T and scaling factor S
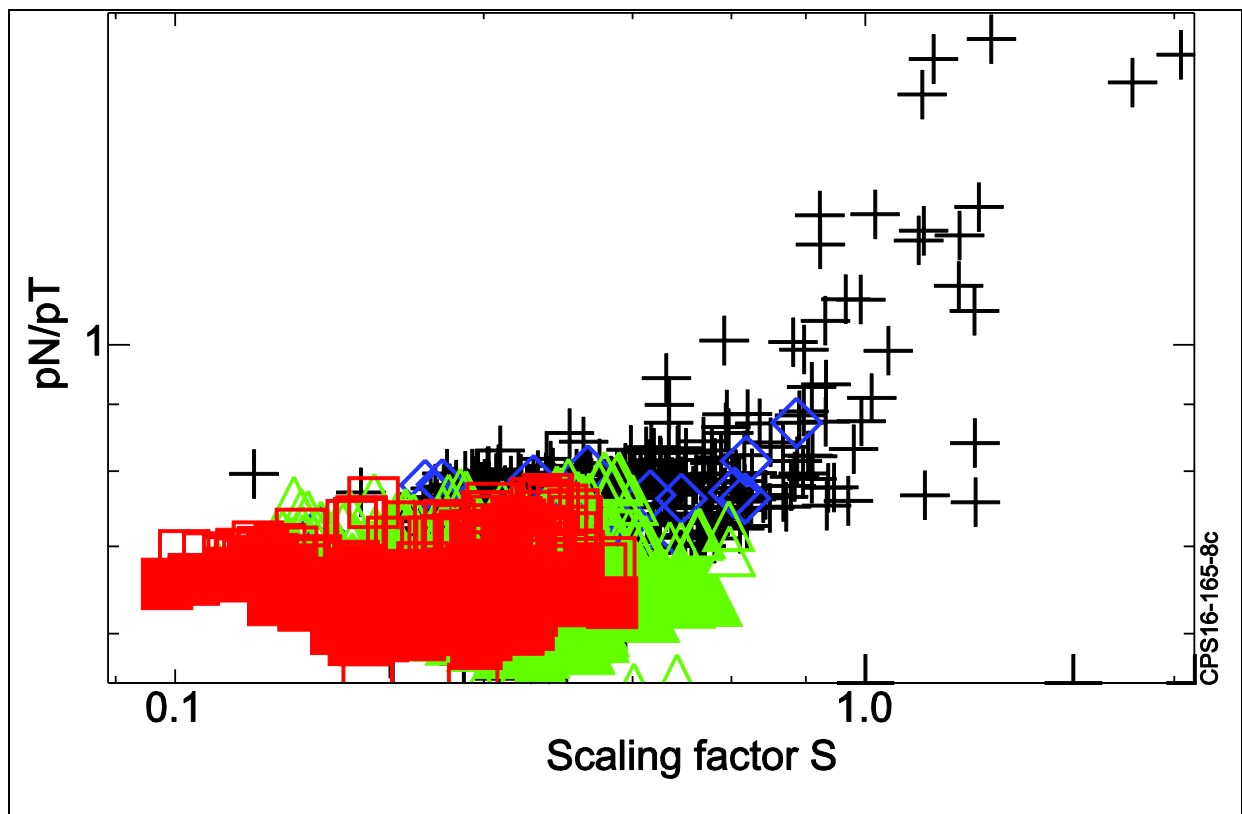
Fig.8. p_N/p_T =(Ne(R_0)/Ne(R_0+0.4m))/(Te(R_0)/Te(R_0+0.4m)) vs. scaling factor S. Colour coding is as in Fig.4: black crosses-P_{RF}/P_{NB}<5%, blue diamonds- 5%<P_{RF}/P_{NB}<10%, green triangles-10%<P_{RF}/P_{NB}<20%, red squares- 20%<P_{RF}/P_{NB}.

A relation between p_N and p_T is shown in Fig.9a. It should be noted that a branch of lower p_N <1 corresponds to initial phase of the pulses with low and rising density. One can notice that a branch with larger peaking p_N =1.2-1.4 is observed in pulses with NB only

18

heating. Noticeably lower density peaking is observed in pulses with combined heating. There is a trend of reduction of p_N at a fixed p_T with increase of $P_{RF}/(P_{RF}+P_{NB})$ as can be seen with a transition from black crosses to red squares. This trend is reflected in the fact that additional anomalous particle pinch is required for a description of the density evolution in NB heated plasma as will be described in section 2. Such pinch should decrease with the rise of P_{RF}/P_{NB}. The pinch variation may occur due to change of the turbulence characteristics depending on the ratio of the electron and ion heating [28],[29]. The temperature peaking p_T increases at a fixed p_N with the rise of P_{RF}/P_{NB} due to central RF heating compared to more peripheral NB heating, especially in pulses with higher densities.

Fig.9b shows a relation between R/L_{Te} and $0.5R/L_{Ne}$, where $R/L_F = F/(dF/dR) \cong$
$(R_0 + R_1)/(R_1 - R_0)(F(R_0) + F(R_1))/(F(R_0) - F(R_1))$, R_0=3.05m, R_1=3.4m. We presume here that general trends in the link between R/L_{Ti} and $0.5R/L_{Nd}$ can be represented by a link between R/L_{Te} and $0.5R/L_{Ne}$. Points corresponding to the scaling factor S>0.8 are shown in Fig.9.b by combined crosses and small orange diamonds. Pronounced radiation peaking caused by central heavy impurity accumulation is observed in a corresponding pulses. According to the neoclassical theory [13] there is a simple relation between impurity convective velocity V_{rz} and diffusion coefficient D_{rz}

$$\frac{RV_{rz}}{D_{rz}} = -Z\left(\frac{R}{L_{ni}} - \frac{R}{2L_{Ti}}\right) \quad (1)$$

in the plasma with a small poloidal asymmetry, the main plasma in the banana and impurity in the Pfirsch-Schluter regimes, where Z is the impurity charge. All points above the diagonal in Fig.9.b correspond to the negative V_r or inward pinch causing the impurity accumulation. No impurity accumulation for outward convection $V_r \propto -R/L_{ne} + R/2L_{Te} > 0$ should be expected below the diagonal in Fig.9b. However, cross-diamonds below the diagonal indicate pulses with central impurity accumulation and the scaling factor S>0.8. Such deviation from

a simple expression (1) is probably connected to the effect of the poloidal asymmetry due to strong toroidal rotation (other causes for the asymmetry such as RF heating could be involved [13],[25]). More general expression for the impurity particle flux has been found in [15,16]:

$$\frac{R\langle\Gamma_z^{neo}\rangle}{\langle n_z\rangle} = q^2 D_c Z \left[\left(\frac{R}{ZL_{nz}} - \frac{R}{L_{ni}} + \frac{R}{2L_{Ti}}\right)P_a - 0.33 P_b f_c \frac{R}{L_{Ti}}\right] \quad (2),$$

where angular brackets denote the flux surface averaging, $D_c = \rho_i^2/\tau_{ii}$ is the diffusion coefficient, $\rho_i^2 = v_{thi}^2/\langle\omega_{ci}^2\rangle$ is the square of averaged Larmor radius,
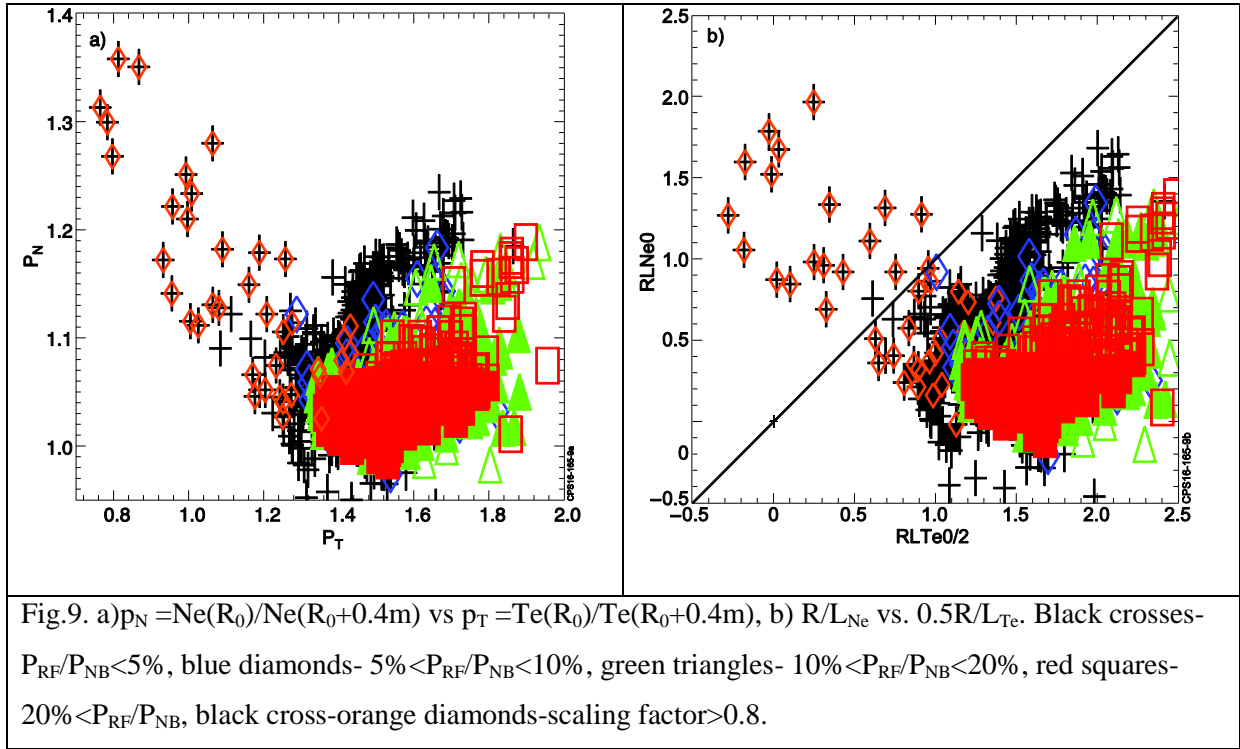
$\tau_{ii} = 3(2\pi)^{3/2}\varepsilon_0^2 m_i^{1/2}T_i^{3/2}/(n_i e^4 \ln\Lambda)$ is a collisional time, q is the safety factor, f_c is a fraction of trapped particles. Parameters $P_{a,b}$ may vary considerably in strongly asymmetric plasma and in the symmetric plasma their values are $P_a = 1$ and $P_b = 0$ [13,14]. The effect of the $P_{a,b}$ variation on the impurity flux is discussed in more detail in the last section of the paper. It should be noted that eqs(1-2) are applicable in the plasma with main ions in the plateau and impurity in the Pfirsch-Schluter regimes.

Analysis of the baseline scenario plasmas shows that the main ions are typically in the plateau regime in the regions either close to the magnetic axis or the plasma edge. Conditions for the banana regime can be fulfilled marginally near the mid radius. The tungsten ions can be in either in the banana ($r/a \leq 0.5$) or PS regime ($r/a \geq 0.5$) assuming that the ionization state is defined by the corona equilibrium. Strictly speaking, eqns.(1-2) are not always applicable in such circumstances. However, one can trace the origin of the term $\dfrac{R}{L_{ni}} - \dfrac{R}{2L_{Ti}}$ in the eqns. (1-2) to the expression for the radial electric field E_r defining the toroidal component of the relative velocity and the friction force between the main ions and impurity. The radial field $E_r = (\partial P_i/\partial r)/(Z_i e n_i) + V_p B_\varphi/c$ is associated with the diamagnetic drift $(\partial P_i/\partial r)/(Z_i e n_i)$ and polodal plasma rotation $V_p = \alpha c(\partial T_i/\partial r)/B_\varphi e Z_i$, where B_φ is the toroidal magnetic field, c-

speed of light, e-electron charge, and Z_i is the main ion charge. Using expression for V_p we have $RE_r eZ_i / T_i = R / L_{ni} - (\alpha - 1)R / L_{Ti}$ (the effect of impurity contribution is neglected here). The coefficient α depends on the plasma collisionality and α=3/2 if the main plasma is in the banana and impurity in PS regimes [13]. The α coefficient will vary with transition of the plasma to a different collisionality regime. The transition will cause a change of the factors in terms proportional to L_{ni}^{-1}, L_{Ti}^{-1} in eqns. (1-2) and L_{nz}^{-1} in eq.(2), but it should not change, presumably, the structure of the eqns.(1-2). A change of the abscissa scale from $R / 2L_{Ti}$ to $(\alpha - 1)R / L_{Ti}$ in Fig.9 would be a consequence of such variation. An investigation of the applicability of eqns.(1-2) in plasmas at different collisionality regimes is being done by S.Citrin, F.J.Casson, C.Bourdelle et al. (private communication).

Fig.9. a)p_N =Ne(R_0)/Ne(R_0+0.4m) vs p_T =Te(R_0)/Te(R_0+0.4m), b) R/L_{Ne} vs. 0.5R/L_{Te}. Black crosses-P_{RF}/P_{NB}<5%, blue diamonds- 5%<P_{RF}/P_{NB}<10%, green triangles- 10%<P_{RF}/P_{NB}<20%, red squares-20%<P_{RF}/P_{NB}, black cross-orange diamonds-scaling factor>0.8.

2. Distinctive features of the JET plasma transport with NB only and combined RF plus NB heating.

To find a plausible interpretation of the trends demonstrated in the previous section we have to emphasise some specific features of the main plasma transport in the baseline scenario pulses with NB only and combined RF plus NB heating. Modelling of JET ILW plasmas have been done using the JETTO [9],[21], code to clarify such features.

The main plasma transport was modelled in the framework of the neoclassical and Bohm/gyro-Bohm [22] model. A pulse with combined RF+NB heating (#85266) was compared to a pulse with NB only heating (#85267). The main plasma parameters are shown in Fig.1 for both pulses. The time interval of the modelled plasma was chosen between t_1=53.5 and t_2=55.3s. Quasi-steady state conditions were observed during this interval in the

pulse with combined RF+NB heating (#86266) and very strong peaking (P_r>10) of the plasma bulk radiation causing disruption (after the end of the interval) was observed in the pulse with NB heating only.

The thermal diffusivities in the plasma core in the modelling were assumed to be a combination of the Bogm, gyro-Bohm and neo-Alcator diffusivities with equal weights [22]. Inside the edge transport barrier the neoclassical diffusivities were enhanced to reproduce the experimental density and temperature at the pedestal. There are two important differences between the two pulses, which find a reflection in the transport coefficient variation. Firstly, in accordance with a general trend demonstrated in Fig.8 and Fig.9a the plasma density is more peaked in a pulse with NB only heating. To match experimental Ne profiles one needs to include anomalous inward pinch in addition to the ware pinch for particles of the main plasma component for pulse #85267. The pinch velocity used in the modelling was chosen in the form $V_{inw} = 0.25 D \Sigma^2 /(V'V_{pl})$, where D is the particle diffusion coefficient and Σ is the flux surface area, $V' = dV(\rho)/d\rho$ and V_{pl} is the plasma volume at $\rho = a$. No pinch is required in the case of combined RF and NB heated plasma (pulse #85266). Secondly, the toroidal plasma rotation is modelled assuming that the toroidal momentum diffusivity is proportional to the ion heat diffusivity with the coefficient of proportionality equal to the Prandtl number N_{pr}. The central plasma rotation has been deduced from the magnetic measurement in the chosen pulses. As was already mentioned earlier the rotation is about 40% larger in the NB only heated plasma. The difference in the rotation frequency is one of the factors causing the difference in the scaling factors in pulses with NB heating only compared to the pulses with the combined heating as shown in in Fig.4-6 and Fig.9. To match the measured and modelled V_{tor} one needs to use N_{pr}=0.4 and 0.65 for the chosen pulses with NB only and RF+NB heating, respectively. The modelled Ne, Te, Ti and Vtor profiles are shown in Fig.10 as compared to the measured profiles (if available). The measured ion temperature is

unavailable for these pulses and the calculated temperature is shown in comparison with electron temperature. Some discrepancy in the peaking of the core density in pulse 85266 is within the error bars of the measurements. A pronounced density peaking was observed in plasmas with high Greenwald fraction $f_{GR} \geq 0.8$ [26]. The Ware pinch and variation in the particle diffusion proportional to the heat diffusivity have been invoked in [26,27] to explain the difference in density peaking found in pulses with combined and NB only heating. Such model, indeed, reasonably well describes the temperature and density evolution in pulse with combined NB and RF heating (#85266) as shown in Fig.10. However, the anomalous pinch is required to match the modelled and measured density profiles in the case of NB only heating (Fig.10, pulse#85267). The anomalous pinch is larger by factor of 2-3 in this case than the Ware pinch in a greater part of the plasma cross section. The relative difference in the heat diffusivities between the two pulses is smaller.

It should be noted that the sawtooth activity was present in all H-mode pulses investigated here. Only the time averaged plasma parameters have been modelled as shown in Fig.10. The averaging has been done over time $\Delta t = 0.2s$ exceeding the period of the sawtooth activity. The effect of the sawtooth activity is hidden in the calculated time averaged diffusivities and convective velocity. It can be different in pulses with different heating methods. Specific role of the sawtooth activity has not been investigated here.
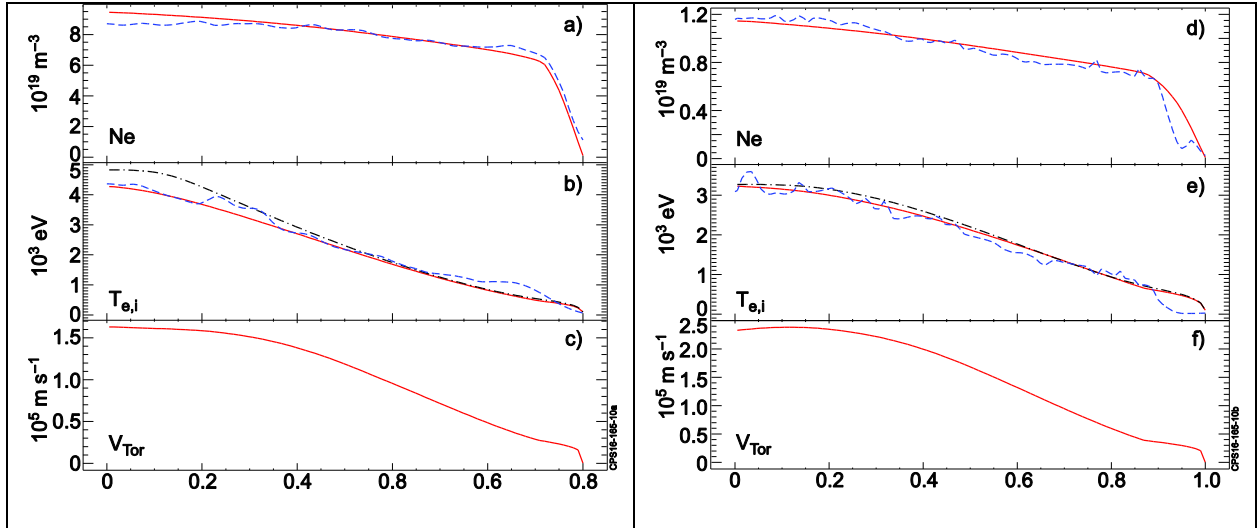
Fig.10. Comparison of modelled and measured profiles of the (a,d)- plasma density Ne, (b,e) -red line-electron and black line- ion temperature, (c,f) -toroidal rotation velocity Vtor. Red and black lines-modelling, blue line measurements. Ti and Vtor measurements are unavailable and modelled Ti profiles are compared with measured Te profiles in panes (b,e). Pulses are (a-c)#85266 and (d-f)#85267 at t=54.5s. The evolution of the main parameters for these pulses is shown in Fig.1. Experimental profiles were averaged over 0.2s.

3. Discussion and conclusions.

Accumulation of tungsten and other heavy impurities (Ni, Cu) has been observed in the core of the plasma with strong toroidal rotation in JET-ILW pulses [1],[2],[3]. A database has been created to find and investigate an empirical trends associated with heavy impurity accumulation. The accumulation causes the plasma radiation peaking (Fig.4) and increase in the radiation fraction $P_R = P_{RAD}/(P_{RF} + P_{NB})$ (Fig.5a). The radiation peaking and the radiation fraction increase with the scaling factor $S = C\omega^2 n /T^{3/2}$ in pulses with NB only heating (Fig.4, Fig.5). A reduction in the energy confinement time (Fig.7) and plasma disruptions caused by cooling of the plasma core by the radiation have been observed in some cases. Largest values of the scaling factor $S = C\omega^2 n /T^{3/2}$ were found in pulses with NB heating only. The largest toroidal rotation was registered also in pulses with NB only heating.

25

Additional RF heating distorts the relation between the radiation fraction and the scaling factor due to increase in the impurity influx from the wall, which rises with RF power (Fig.5). The radiation becomes more peripheral in pulses with the combined heating (Fig.5b) and less harmful as it cause neither significant radiative cooling of the plasma core nor the plasma disruption.

The impurity accumulation and radiation peaking depend on the plasma rotation ω and peaking of the main plasma density and temperature (eq.(1)). Transport modelling demonstrates that temperature evolution is well described in the framework of the Bohm/gyro-Bohm model. The anomalous particle pinch, according to the modelling, causes the main plasma density peaking in NB only heated plasmas (see section 2 and Fig.10). The peaking and the pinch are decreasing in the case of the combined heating with the rise of P_{RF}/P_{NB}. Enhanced momentum diffusivity (Prandtl number) explains smaller plasma toroidal rotation in the presence of the RF power compared to NB only heated cases. The rotation is slowed down (Prandtl number increases) with the rise of the RF power.

Three important factors cause a difference in the impurity accumulation in pulses with NB only compared to combined NB and RF heating: (1) the plasma rotation is larger in pulses with NB heating only due to smaller momentum diffusivity (section 2). (2) the main plasma density peaking is stronger due to larger anomalous particle pinch and (3) the temperature peaking is weaker due to more peripheral heating in pulses with NB only heating compared to combined NB and RF heating cases (Fig.8 and section2). The relative density to temperature peaking $N_p/T_p=(Ne(R_0)/Ne(R_0+0.4m))/(T_e(R_0)/T_e(R_0+0.4m))$ is larger in NB only heated plasma (Fig.9).

Observed heavy impurity accumulation is consistent, qualitatively, with the neoclassical theory [13],[14],[15],[23],[24]. The theory predicts (eq.(1)) that the impurity convective velocity V_r is proportional to the parameter $R/L_n-0.5R/L_T$ in the plasma with the

26

main ions in the banana and impurity ions in the Pfirsch-Schluter regimes in the absence of strong poloidal asymmetry. Fig.9a shows that the sign of the velocity V_r deviates from prediction based on eq.(1). The deviation is caused by the poloidal asymmetry due to fast plasma toroidal rotation. Other possible causes of the asymmetry may include RF heating [13],[25]. Eq.(1) is modified to eq.(2) for the particle flux of the impurity in the presence of the asymmetry. A simple empirical scaling parameter S demonstrated in fig.4 and Fig.5 allows a relatively accurate prediction of the heavy impurity accumulation in JET H-mode plasmas with toroidal rotation avoiding more complicated calculation of the parameters f_c and Pa,b in eq.(2).

The scaling factor S= $C\omega^2 n_D / T_D^{3/2}$ in the empirical trends demonstrated in Fig.4-6 and Fig.8 reflects a dependence of the friction force F_c between the impurity and the main plasma ions on the collisional frequency $v^{W/D} \propto n_D / T_D^{3/2}$. The friction force component parallel to the magnetic field $F_{c//}$ gives rise to the radial neoclassical transport of the impurity. Such transport is proportional, according to eqs.(1,2), to the impurity ion charge Z and radial electric field due to the diamagnetic drift and the poloidal rotation $E_r \propto R(1/L_{ni} - R/2L_{Ti})$ in the plasma with weak poloidal asymmetry. The factors $P_A = \langle B^2 \rangle / \langle n_z \rangle \left[\langle n_z / B^2 \rangle - 1/\langle B^2 / n_z \rangle \right] / 2\varepsilon^2$ and $P_B = \langle B^2 \rangle / \langle n_z \rangle \left[\langle n_z \rangle / \langle B^2 \rangle - 1/\langle B^2 / n_z \rangle \right] / 2\varepsilon^2$ in eq.(2) change from $P_A=1$ and $P_B=0$ in the absence of the asymmetry to $P_A=P_B=1/2\varepsilon^2$ in the limit of infinite poloidal localization of the impurity [13,14], when $n_z(\theta) \to \delta(\theta)$, where θ is the poloidal angle and δ is the delta function and ε=ρ/R. Such strong variation of the P_A and P_B with transition from poloidally symmetric to asymmetric impurity distribution associated with toroidal rotation may cause a considerable change of the impurity particle flux $R\langle \Gamma_z^{neo} \rangle / \langle n_z \rangle$ in eq.(2). The dependence of the scaling factor S on ω^2 should occur due to poloidal inhomogeneity of the impurity. The inhomogeneity is caused by the centrifugal

force due to toroidal plasma rotation and it is proportional to ω^2. It has been shown in ref. [30] that the impurity pinch velocity is proportional to the factor of ω^2 in the plasma with a strong poloidal asymmetry.

The sawtooth activity was observed in all H-mode pulses in the database. Analysed parameters were averaged over time exceeding a period of the activity. It should be noted, however, that the period, the inversion radius and the amplitude of density and temperature oscillations caused by the activity may depend on the heating method. Specific role of the sawtooth activity has not been analysed here.

References

[1] Y.Baranov et al "Interplay between confinement, impurities and MHD in JET Hybrid pulses with ITER like wall" 40th EPS conference on Plasma Physics, Espoo, Finland 2013

[2] C.Angioni et al "Neoclassical and turbulent transport of W in toroidally rotating JET plasmas" 40th EPS conference on Plasma Physics, Espoo, Finland 2013

[3] P.Mantica et al "Transport analysis of Tungsten and Beryllium in JET Hybrid Plasmas with the ITER-like wall" 40th EPS conference on Plasma Physics, Espoo, Finland 2013

[4] R. Neu, et al., Phys. Plasmas 20, 056111 (2013).

[5] T. Püetterich et al, "Taming Tungsten in JET and ASDEX Upgrade" 40th EPS conference on Plasma Physics, Espoo, Finland 2013

[6] C. Giroud et al Nucl.Fusion **53** (2013) 113025

[7] G.J. van Rooij, et al, Journal of Nuclear Materials 438 (2013) S42–S47

[8] V. Parail et al J.Nucl.Mater. "Coupled core-SOL modelling of Wcontamination in H-mode JET plasmas with ITER-like wall" 2014

[9] M. Romanelli et al. Plasma and Fusion Res. Volume 9, 3403023 (2014)

[10] C. Angioni et al 2014 Nucl. Fusion 54 083028

[11] F.L.Hinton, S.K.Wong Phys. Fluids 28 (1985) 3082

[12] E.A. Belli et al Plasma Phys. Control. Fusion 124002 (2014)

[13] C. Angioni, F.Casson et all, Physics of Plasmas 22, 055902 (2015) "The impact of poloidal asymmetries on tungsten transport in the core of JET H-mode plasmas"

[14] C Angioni and P Helander Plasma Phys. Control. Fusion 56 (2014) 124001 (7pp) "Neoclassical transport of heavy impurities with poloidally asymmetric density distribution in tokamaks"

[15] E A Belli and J Candy, Plasma Phys. Control. Fusion 57 (2015) 054012 (11pp) "Neoclassical transport in toroidal plasmas with nonaxisymmetric flux surfaces"

[16] Belli E. and Candy J. 2008 Plasma Physics and Controlled Fusion 50 095010, 2012 Plasma Physics and Controlled Fusion 54 015015

[17] Casson F. J. et al. Phys. Plasmas **17**, 102305 (2010)

[18] Peeters A.G. et al 2009 Computer Physics Communications 180 2650

[19] E. Lerche, et al., "ICRH for mitigation of core impurity accumulation in JET-ILW", Proceedings of the 25th IAEA Fusion Energy Conference, 2015, St-Petersburg, Russia, EX/P5-22.

[20] Vl. Bobkov, et al., Journal of Nuclear Materials 438 (2013) S160–S165

[21] G. Cenacchi, A. Taroni, "JETTO: A free boundary plasma transport code", 1988, JETIR (88) 03

[22] L. Garzotti, et al, Nucl. Fusion 43 (2003) 1829–1836

[23] F.L.Hinton, R.D.Hazeltine Rev.Mod.Phys 48 1976 239

[24] S.P.Hirshman, D.J.Sigmar Nucl.Fusion 21 1981 1079

[25] F. J. Casson, et al, "Theoretical description of heavy impurity transport and its application to the modelling of tungsten in JET and ASDEX upgrade" Plasma Phys. Control. Fusion 57 2015 014031.

[26] J. Stober, et al, Plasma Phys. Control. Fusion **43** (2001) A39–A53

[27] C. Giroud, et al, Plasma Phys. Control. Fusion **57** (2015) 035004

[28] E. Fable, et al, Plasma Phys. Control. Fusion **52** (2010) 015007

[29] C. Angioni, et al, Nucl. Fusion 52 (2012) 114003

[30] M Romanelli et a., Plasma Phys. Control. Fusion **40** (1998) 1767